

Supplementary Information “Hybrid data-model driven prediction of soil thickness in a mountainous watershed”

Qina Yan¹, Haruko Wainwright¹, Baptiste Dafflon¹, Sebastian Uhlemann¹, Carl I. Steefel¹, Nicola Falco¹, Jeffrey Kwang², Susan S. Hubbard¹

5 ¹Earth and Environmental Science Area, Lawrence Berkeley National Laboratory, Berkeley, CA., USA.

² Department of Geosciences, University of Massachusetts Amherst, Amherst, MA, USA.

Correspondence to: Qina Yan (qinayan@lbl.gov); Haruko Wainwright (HMWainwright@lbl.gov)

10 Posterior distribution of the parameters

We used the Bayesian method to calculate the posterior distribution of the parameters in this hybrid-model (Eqn. 6-8) and estimated the maximum a posteriori (MAP).

15 The parameter set is defined as a vector θ , including six parameters (except for K_s in Eqn. 3b). We define the prior distribution for θ , $p(\theta)$, which is the products of independent uniform distributions for the parameters. We define the real soil thickness data vector \mathbf{z} (which is a m -vector with m field sampling points: $\{z_1, z_2, \dots, z_m\}$) as the sum of predicted soil thickness and error vector $\boldsymbol{\varepsilon}$:

$$\mathbf{z} = \mathbf{y} + \boldsymbol{\varepsilon} \quad (\text{S1})$$

20 where \mathbf{y} is the predicted soil thickness based on the parameter sets:

$$\mathbf{y} = f(\theta). \quad (\text{S2})$$

We assume that each element in the error vector follows a normal distribution with a standard deviation σ . We estimate the standard deviation of the measurement error based on the discrepancy between the auger and CPT measurements.

25 Using the Bayes' rule, we define the posterior distribution as:

$$p(\theta|\mathbf{z}) \propto p(\mathbf{z}|\theta)p(\theta) \quad (\text{S3})$$

Since the error vector is normal, the likelihood $p(\mathbf{z}|\theta)$ is a normal distribution.

30 To compute the posterior distribution, we use the sampling-resampling scheme (Smith and Gelfand, 1992). We sample the parameter set at each grid following the grid search $\{\theta^{(1)}, \theta^{(2)}, \dots, \theta^{(N)}\}$, where $N = 6^6 = 46656$ and predict the soil thickness at the measurement locations $\{\mathbf{y}^{(1)}, \mathbf{y}^{(2)}, \dots, \mathbf{y}^{(N)}\}$ where $\mathbf{y}^{(i)} = f(\theta^{(i)})$

$$p(\theta = \theta^{(i)}|\mathbf{z}) = \frac{l^{(i)}}{\sum_{j=1}^N l^{(j)}} \quad (\text{S4})$$

35 $p(\theta|\mathbf{z})$ = distribution

$$\mathbf{y}^{(1)} = \{y_1^{(1)}, \dots, y_m^{(1)}\}$$

40 Where the likelihood $l^{(i)}$ is defined as the normal distribution with the mean $\mathbf{y}^{(i)}$ and the standard deviation σ as:

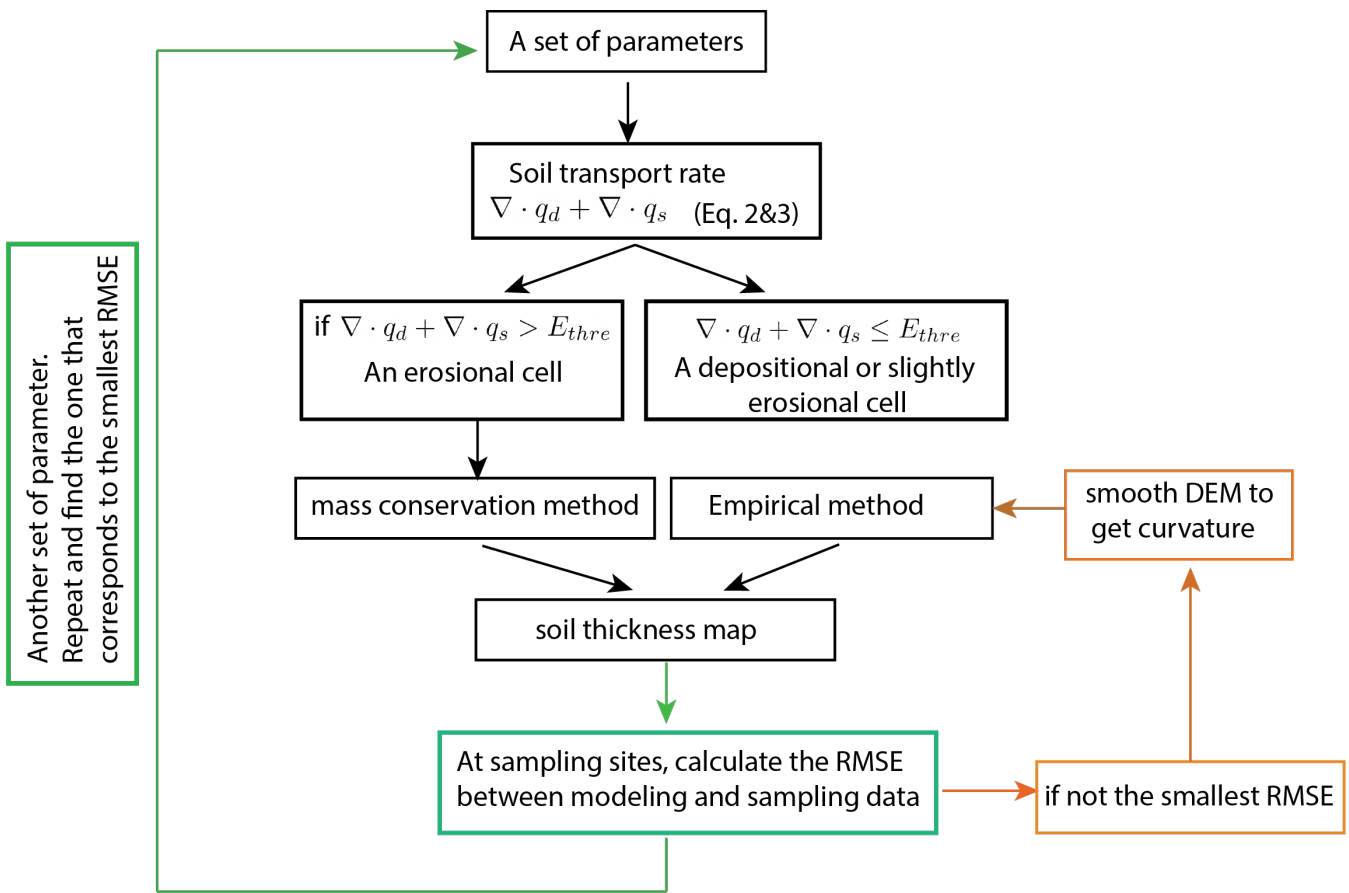
$$l^{(i)} = N(\mathbf{z} - \mathbf{y}^{(i)}, \sigma)$$
$$l^{(i)} = N(z_1 - y_1^{(i)}, \sigma) \dots N(z_m - y_m^{(i)}, \sigma) \quad (\text{S5})$$

45 Since we assume that each data point ($j = 1 \dots m$) is independent, we can represent the likelihood as the product of normal distributions of individual measurements.

$$l^{(i)} = C \prod_{j=1}^m \exp \left[-\frac{(z_j - y_j^{(i)})^2}{2\sigma^2} \right] = C \exp \left[\sum_{j=1}^m -\frac{(z_j - y_j^{(i)})^2}{2\sigma^2} \right]$$
$$\hat{l}^{(i)} = \operatorname{argmax} \left\{ C \exp \left[\sum_{j=1}^m -\frac{(z_j - y_j^{(i)})^2}{2\sigma^2} \right] \right\}$$

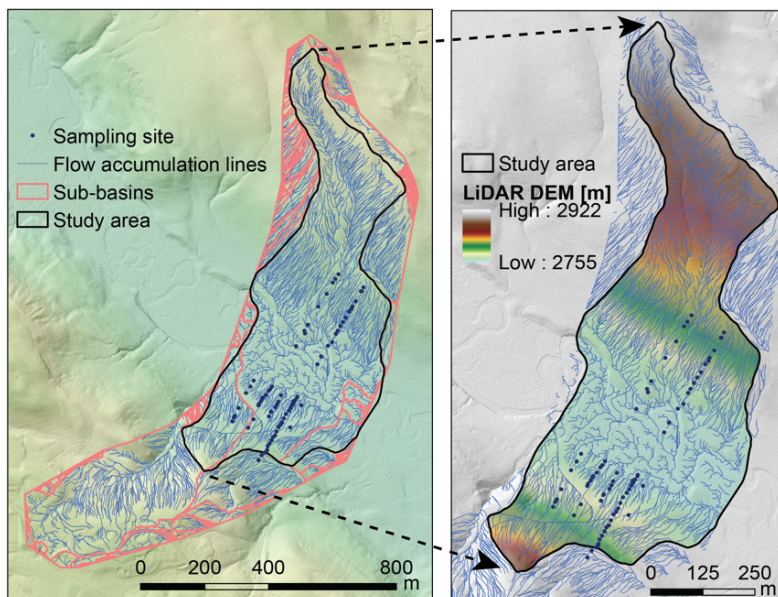
50 Note that C is the normalization factor. The standard deviation of the error is equal to the standard deviation of the difference. We then obtained the MAP estimate as the parameter set that provides the maximum posterior probability. The marginal distribution of each parameter can be calculated by the summation of the posterior distributions given each fixed parameter value (Fig. S8). (S6)

55

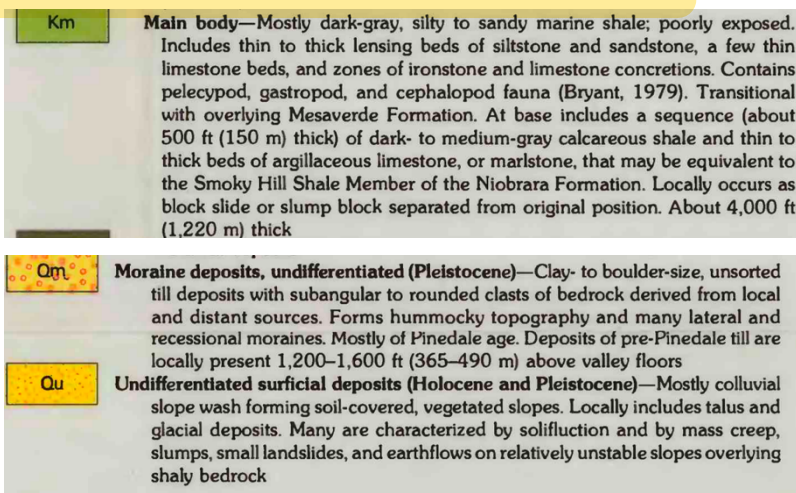
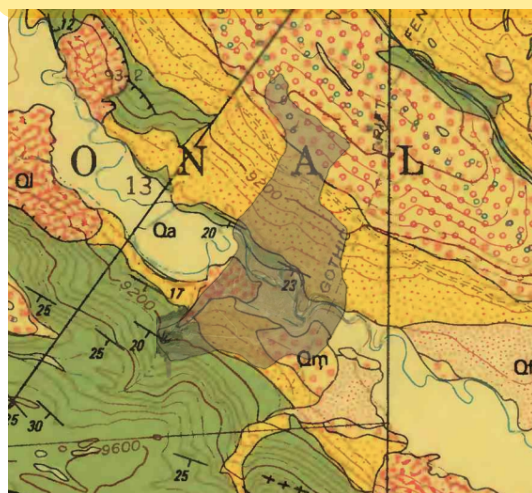


60

Figure S1: The workflow of the hybrid method.



65 **Figure S2: Drainage area delineation.** The drainage areas are created by locating the pour points at the edges of the analysis window (where water would pour out of the raster), as well as sinks, then identifying the contributing area above each pour point.



70 **Figure S3: A geological map of parent materials and deposits.**



Figure S4: Field images of saprolite layers from auger sampling.

75

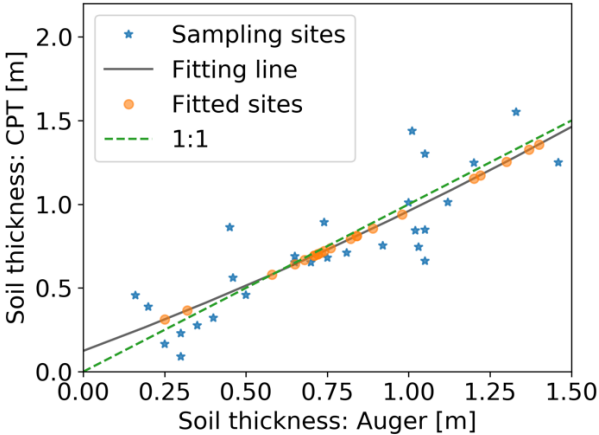
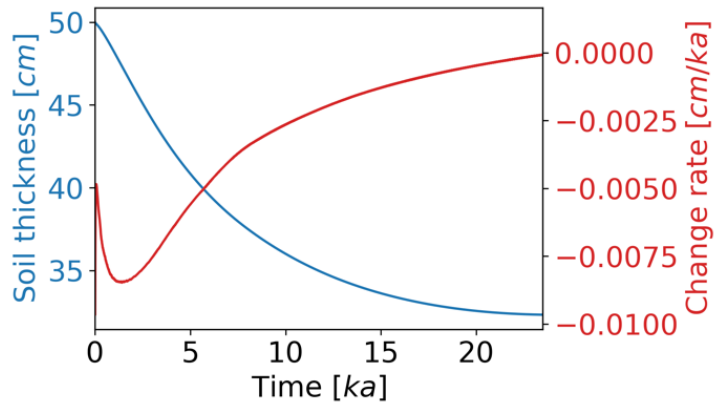


Figure S5: Fitting the soil thickness of the CPT data using the auger data. Correlation = 0.86, Root-minimum-square-error = 0.20 m.

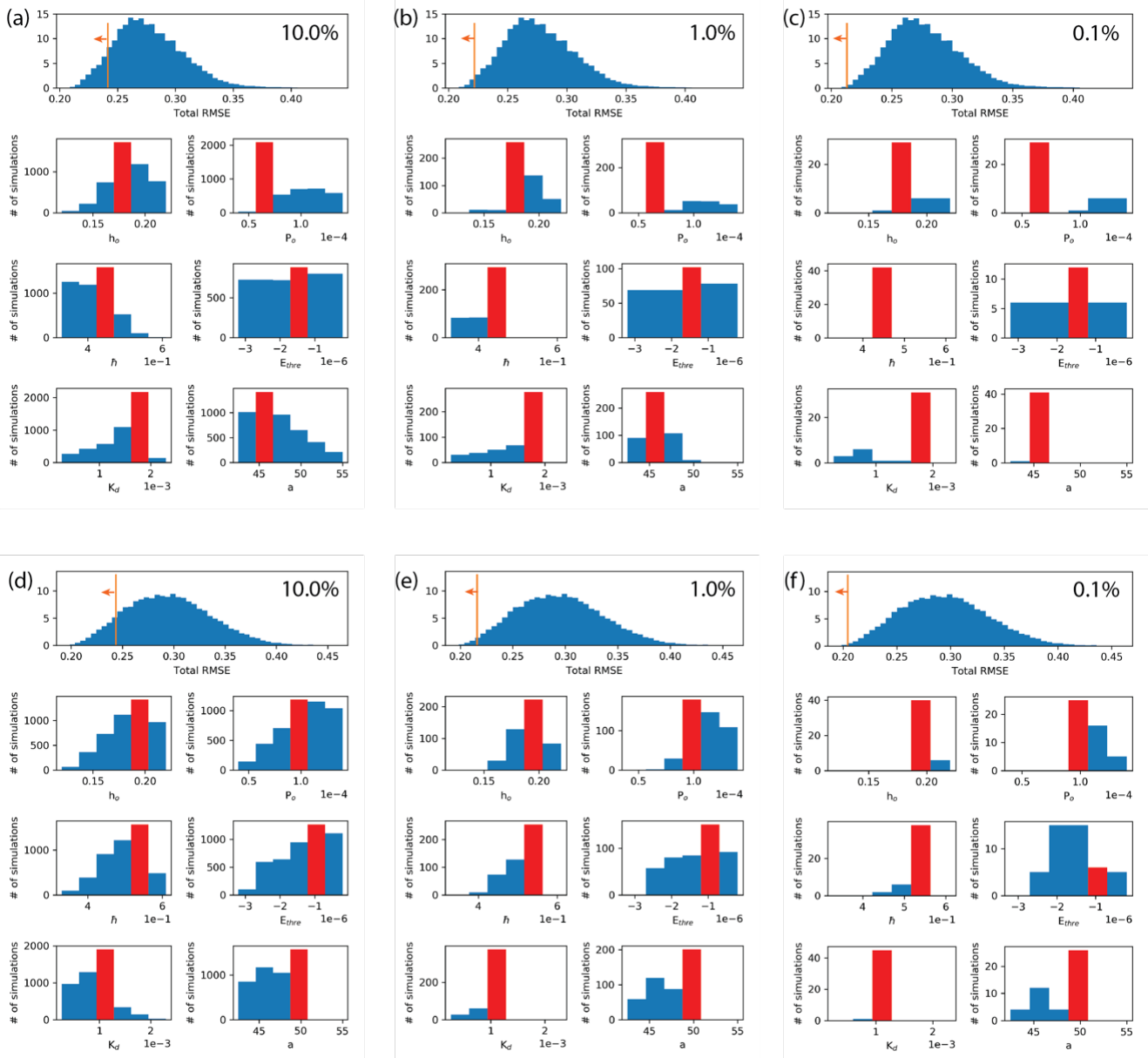
80

85



90

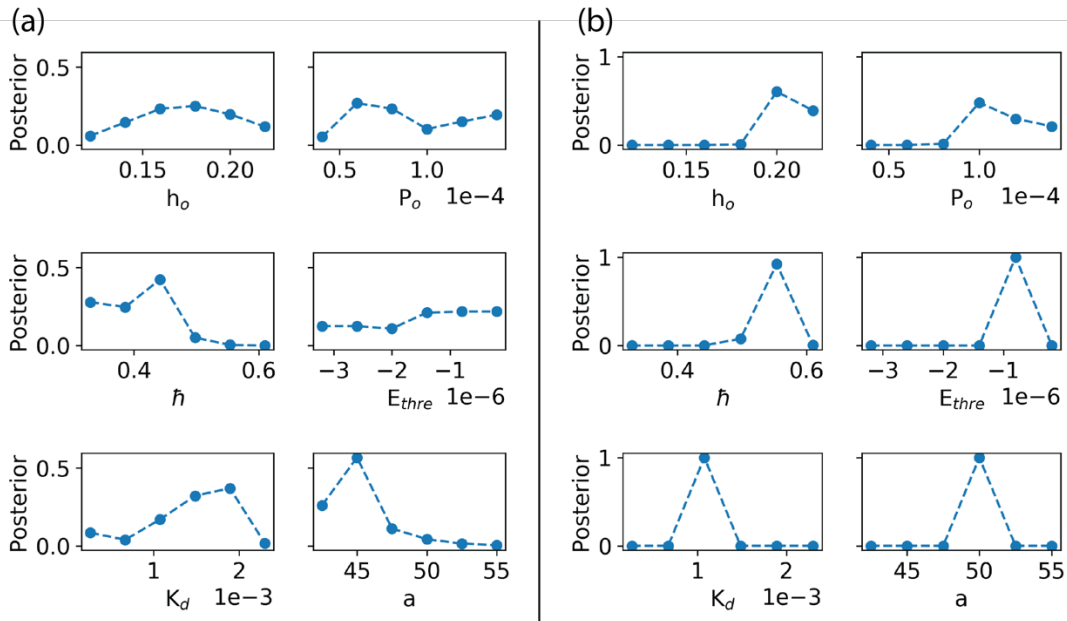
Figure S6: Spatial mean values of erosional sites of soil thickness evolution over time. The initial soil thickness is 0.5 m, time step is 1 year, and the initial elevation is the current DEM data. The boundary condition is Neumann boundary condition, the surface transport fluxes around the edge is zero. The time step is 1 yr, and the diffusion coefficient is $1.1 \times 10^{-3} \text{ m}^2/\text{yr}$ for the north-facing hillslope and $1.8 \times 10^{-3} \text{ m}^2/\text{yr}$ for the south-facing hillslope.



95

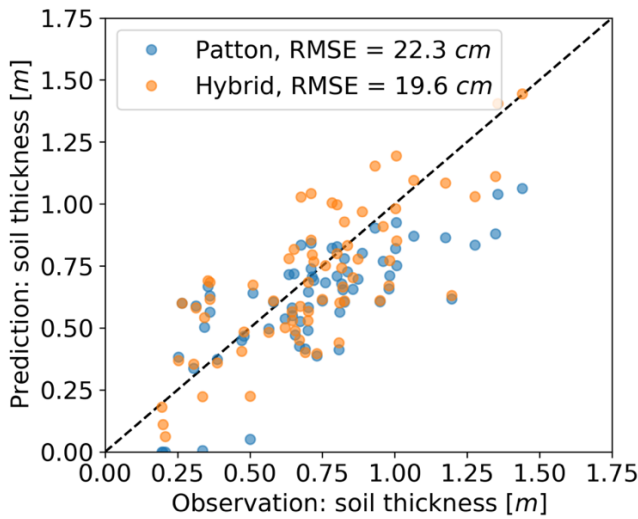
00

Figure S7: Probability density function and histogram plots from a series of simulations of a grid search. The root-mean-square error (RMSE) between the simulated and measured soil thickness. (a-c) The RMSE for the south-facing hillslope and the corresponding histogram plots which show the distribution of each parameter that corresponds to 10.0%, 1.0%, and 0.1% of the smallest RMSE values, respectively; (d-f) The RMSE of north-facing hillslope and the corresponding histogram plots which show the distribution of each parameter that corresponds to 10.0%, 1.0%, and 0.1% of the smallest RMSE values, respectively. The red color bar represents the parameter that provides the global minimum between simulation and field measurement.



05

Figure S8: Marginal posterior probabilities of six parameters. (a) The posterior probabilities of the six parameters for the south-facing hillslope; (b) The posterior probabilities of the six parameters for the north-facing hillslope.



10

Figure S9: Parameter calibrations for the hybrid model. The root-mean-square error (RMSE) and Pearson's correlation between sampling and simulation results are calculated for the south-facing (a) and north-facing (b), respectively.

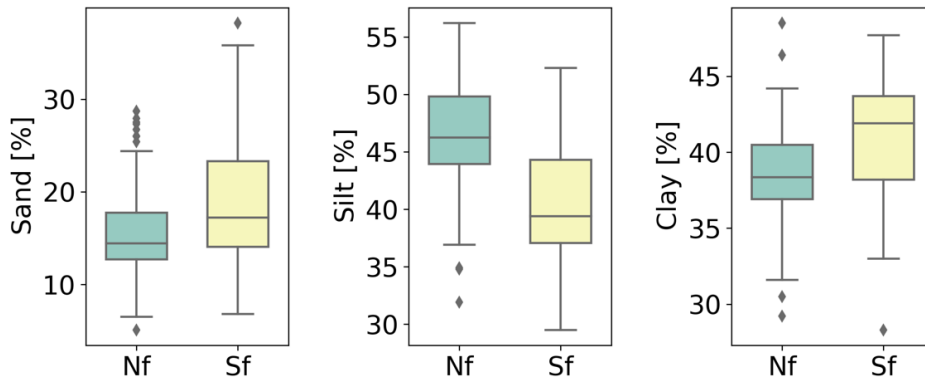


Figure S10: Soil texture at two hillslopes. Nf = North-facing hillslope, Sf = South-facing hillslope.

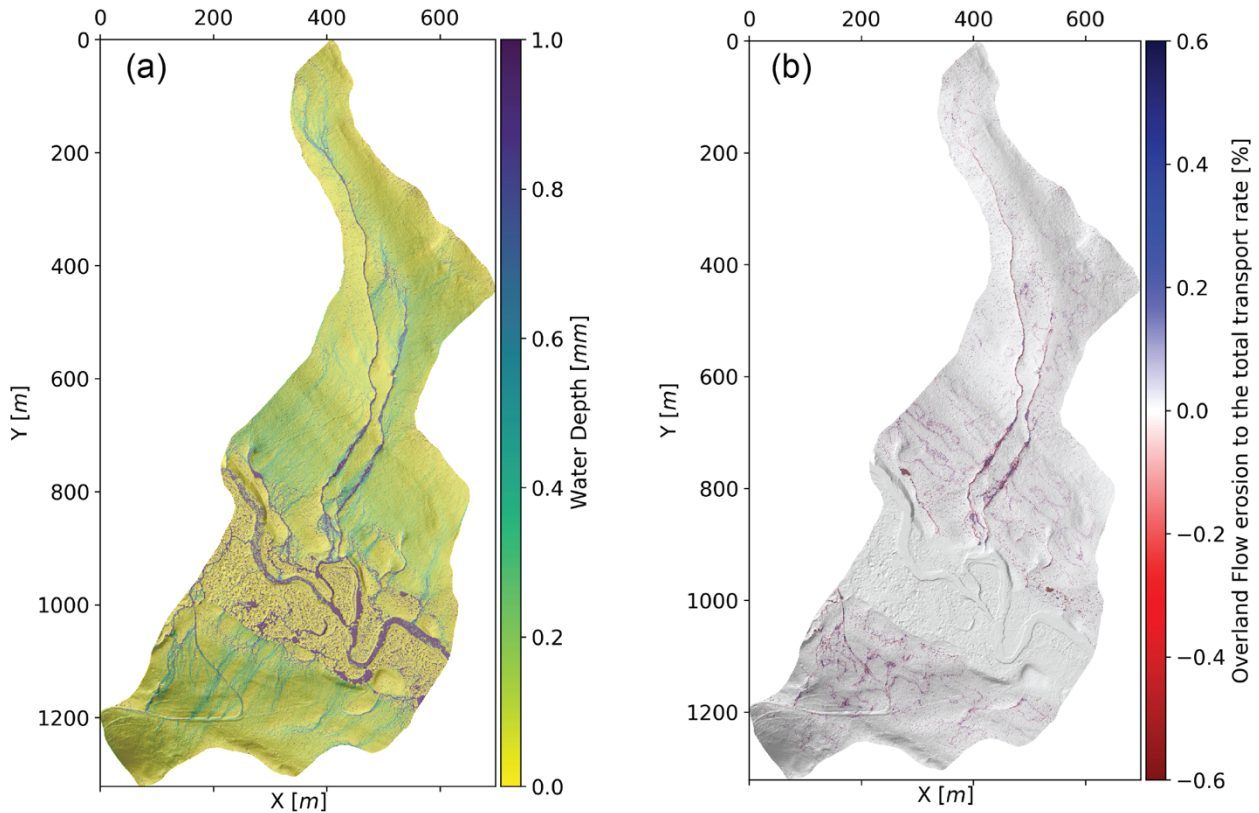


Figure S11: (a) water depth of overland flow at a steady-state, which occurs after 6 days with constant rainfall = 363 mm/yr, and the time step $\Delta t \approx 1\text{sec}$; (b) The rate of the overland flow erosion rate to the total soil transport rate. The overland flow erosion mechanism is from Equation 3.

25 **Table S1. A list of topographic variables for the correlation with soil thickness:**

| Variable names | Explanation |
|------------------------|--|
| Lidar_2018_Aspect_NEON | Topographical aspect computed at the original pixel resolution of 1m |
| Aspect_NEON_10m | Topographical aspect computed at a pixel resolution of 10m |
| Aspect_NEON_10m_x3 | Topographical aspect computed at a pixel resolution of 10m and smoothed considering a 3x3-pixel moving window |
| Aspect_NEON_10m_x5 | Topographical aspect computed at a pixel resolution of 10m and smoothed considering a 5x5-pixel moving window |
| Aspect_NEON_10m_x9 | Topographical aspect computed at a pixel resolution of 10m and smoothed considering a 9x9-pixel moving window |
| C_unc | Uncertainty of the estimated leaf carbon content derived by airborne hyperspectral data (pixel resolution of 1 m) |
| C | Leaf carbon content derived by airborne hyperspectral data (pixel resolution of 1 m) |
| N_unc | Uncertainty of the estimated leaf nitrogen content derived by airborne hyperspectral data (pixel resolution of 1 m) |
| N | Leaf nitrogen content derived by airborne hyperspectral data (pixel resolution of 1 m) |
| CN_unc | Uncertainty of the estimated leaf carbon/nitrogen ratio derived by airborne hyperspectral data (pixel resolution of 1 m) |
| CN | Leaf carbon/nitrogen derived by airborne hyperspectral data (pixel resolution of 1 m) |
| chm_mosaic | Canopy height model (i.e., plant height) at 1 m pixel resolution |
| LMA | Leaf mass area derived by airborne hyperspectral data (pixel resolution of 1 m) |
| LMA_unc | Uncertainty of the estimated leaf mass area derived by airborne hyperspectral data (pixel resolution of 1 m) |
| LWC | Leaf water content derived by airborne hyperspectral data (pixel resolution of 1 m) |
| Curv_NEON_10m | Topographical curvature computed at a pixel resolution or 10m |
| Curv_NEON_10m_x3 | Topographical curvature computed at a pixel resolution or 10m and smoothed considering a 3x3-pixel moving window |
| Curv_NEON_10m_x5 | Topographical curvature computed at a pixel resolution or 10m and smoothed considering a 5x5-pixel moving window |
| Curv_NEON_10m_x9 | Topographical curvature computed at a pixel resolution or 10m and smoothed considering a 9x9-pixel moving window |
| dsm_mosaic | Digital surface model at 1 m resolution |
| dsm_mosaic_10m | Digital surface model at 10 m resolution |
| dtm_mosaic | Digital terrain model at 1 m resolution |

| | |
|-----------------------|--|
| dtm_mosaic_10m | Digital terrain model at 10 m resolution |
| FlowAcc_NEON | Topographical flow accumulation computed at the original pixel resolution of 1m |
| FlowAcc_NEON_10m | Topographical flow accumulation computed at a pixel resolution of 10m |
| FlowAcc_NEON_10m_x3 | Topographical flow accumulation computed at a pixel resolution of 10m and smoothed considering a 3x3-pixel moving window |
| FlowAcc_NEON_10m_x5 | Topographical flow accumulation computed at a pixel resolution of 10m and smoothed considering a 5x5-pixel moving window |
| FlowAcc_NEON_10m_x9 | Topographical flow accumulation computed at a pixel resolution of 10m and smoothed considering a 9x9-pixel moving window |
| NEON_mosaic_NDNI | Normalized difference nitrogen index computed from the airborne hyperspectral data |
| NEON_mosaic_NDVI | Normalized difference vegetation index computed from the airborne hyperspectral data |
| NEON_mosaic_NDWI | Normalized difference water index computed from the airborne hyperspectral data |
| NEON_mosaic_liq_water | Canopy water content estimated from the airborne hyperspectral data |
| SlopeDeg_NEON | Topographical aspect computed at the original pixel resolution of 1m |
| SlopeDeg_NEON_x3 | Topographical slope in degree computed at a pixel resolution of 1m and smoothed considering a 3x3-pixel moving window |
| SlopeDeg_NEON_x9 | Topographical slope in degree computed at a pixel resolution of 1m and smoothed considering a 9x9-pixel moving window |
| SlopeDeg_NEON_10m | Topographical slope in degree computed at a pixel resolution of 10m |
| SlopeDeg_NEON_10m_x3 | Topographical slope in degree computed at a pixel resolution of 10m and smoothed considering a 3x3-pixel moving window |
| SlopeDeg_NEON_10m_x5 | Topographical slope in degree computed at a pixel resolution of 10m and smoothed considering a 5x5-pixel moving window |
| SlopeDeg_NEON_10m_x9 | Topographical slope in degree computed at a pixel resolution of 10m and smoothed considering a 9x9-pixel moving window |
| Srad_10m | Solar radiation computed at a pixel resolution of 10m. |
| TPI_NEON_10m_x3 | Topographical position index computed at a pixel resolution of 10m and smoothed considering a 3x3-pixel moving window |
| TPI_NEON_10m_x5 | Topographical position index computed at a pixel resolution of 10m and smoothed considering a 5x5-pixel moving window |
| TPI_NEON_10m_x9 | Topographical position index computed at a pixel resolution of 10m and smoothed considering a 9x9-pixel moving window |
| TWI_NEON_10m | Topographical wetness index computed at a pixel resolution of 10m |
| TWI_NEON_10m_x3 | Topographical wetness index computed at a pixel resolution of 10m and smoothed considering a 3x3-pixel moving window |

| | |
|---------------------|--|
| TWI_NEON_10m_x5 | Topographical wetness index computed at a pixel resolution of 10m and smoothed considering a 5x5-pixel moving window |
| TWI_NEON_10m_x9 | Topographical wetness index computed at a pixel resolution of 10m and smoothed considering a 9x9-pixel moving window |
| UPslope_NEON_10m | local upslope drainage area computed at a pixel resolution of 10m |
| UPslope_NEON_10m_x3 | local upslope drainage area computed at a pixel resolution of 10m and smoothed considering a 3x3-pixel moving window |
| UPslope_NEON_10m_x5 | local upslope drainage area computed at a pixel resolution of 10m and smoothed considering a 5x5-pixel moving window |
| UPslope_NEON_10m_x9 | local upslope drainage area computed at a pixel resolution of 10m and smoothed considering a 9x9-pixel moving window |

References

- 30 A. F. M. Smith and A. E. Gelfand, Bayesian statistics without tears: a sampling-resampling perspective, Am. Statistician, 46 (1992), pp. 84–88.